

Effective spin distribution of black hole mergers in triples

Giacomo Fragione^{1,2*}, Bence Kocsis³

¹*Department of Physics & Astronomy, Northwestern University, Evanston, IL 60202, USA*

²*Center for Interdisciplinary Exploration & Research in Astrophysics (CIERA), Evanston, IL 60202, USA*

³*Institute of Physics, Eötvös University, Pázmány P. s. 1/A, Budapest, 1117, Hungary*

14 February 2020

ABSTRACT

Many astrophysical scenarios have been proposed to explain the several black hole (BH) and neutron star binary mergers observed via gravitational waves (GWs) by the LIGO-Virgo collaboration. Contributions from various channels can be statistically disentangled by mass, spin, eccentricity and redshift distributions of merging binaries. In this paper, we investigate the signatures of BH-BH binary mergers induced by a third companion through the Lidov-Kozai mechanism in triple systems. We adopt different prescriptions for the supernovae natal kicks and consider different progenitor metallicities and initial orbital parameters. We show that the typical eccentricity in the LIGO band is 0.01-0.1 and that the merger rate is in the range $0.008 - 9 \text{ Gpc}^{-3} \text{ yr}^{-1}$, depending on the natal kick prescriptions and progenitor metallicity. Furthermore, we find that the typical distribution of effective projected spin is peaked at $\chi_{\text{eff}} \sim 0$ with significant tails. We show that the triple scenario could reproduce the distribution of χ_{eff} . We find that the triple channel may be strongly constrained by the misalignment angle between the binary component spins in future detections with spin precession.

Key words: galaxies: kinematics and dynamics – stars: black holes – stars: neutron – stars: kinematics and dynamics – Galaxy: kinematics and dynamics

1 INTRODUCTION

Many astrophysical scenarios have been proposed to explain the several black hole (BH) and neutron star (NS) binary mergers observed via gravitational wave (GW) emission by the LIGO-Virgo collaboration. Possibilities include isolated binary evolution (Belczynski et al. 2016; Kruckow et al. 2018), mergers catalyzed by stellar envelope expansion (Tagawa et al. 2018), mergers in star clusters (Askar et al. 2017; Banerjee 2018; Fragione & Kocsis 2018; Rodriguez et al. 2018), mergers in galactic nuclei (O’Leary et al. 2009; Antonini & Perets 2012; Fragione et al. 2019; Grishin et al. 2018; Hamilton & Rafikov 2019; Rasskazov & Kocsis 2019), mergers in gaseous disks (Bartos et al. 2017; Stone et al. 2017; Tagawa et al. 2019), and Lidov-Kozai (LK) mergers in isolated triple and quadruple systems (Antonini et al. 2017; Silsbee & Tremaine 2017; Arca-Sedda et al. 2018; Fragione & Kocsis 2019; Liu & Lai 2019).

With the improving sensitivity of LIGO-Virgo and the expected commissioning of KAGRA and LIGO India, hundreds of detections of merging systems is expected within the decade. Thus, it is fundamental to provide tools to distinguish among the mergers that originate in different astrophysical channels. It has been shown that useful parameters

that can help doing so are the masses, spins, eccentricity and redshift of the merging binaries. Their distributions can be used as an indicator to statistically disentangle among the contributions of the several scenarios. This includes identifying correlations between mass and eccentricity (Breivik et al. 2016; Gondán et al. 2018), mass and spins (Postnov & Kuranov 2017; Arca Sedda & Benacquista 2019a; Yang et al. 2019), the mass distribution (Stevenson et al. 2015; O’Leary et al. 2016; Fishbach et al. 2017; Zevin et al. 2017; Mandel et al. 2017; Kocsis et al. 2018; Perna et al. 2019; Yang et al. 2019), the spin distribution (Fishbach et al. 2017), eccentricity distribution in the LIGO/Virgo band (Wen 2003; O’Leary et al. 2009; Cholis et al. 2016; Arca-Sedda et al. 2018; Gondán et al. 2018; Samsing et al. 2018; Zevin et al. 2018) and in the LISA band (O’Leary et al. 2006; Nishizawa et al. 2016, 2017; D’Orazio & Samsing 2018; Samsing & D’Orazio 2018), spin orientations (Rodriguez et al. 2016; Stevenson et al. 2017; Talbot & Thrane 2017; Vitale et al. 2017; Liu & Lai 2017, 2018; Farr et al. 2018; Gerosa et al. 2018; Liu & Lai 2018; Lopez et al. 2018), the projected effective spin parameter (Antonini et al. 2018; Ng et al. 2018; Schröder et al. 2018; Zaldarriaga et al. 2018), and other waveform features (Meiron et al. 2017; Inayoshi et al. 2017; Samsing et al. 2018; Kremer et al. 2018; Samsing et al. 2019).

GW emission is highly efficient at circularizing the orbit of an inspiraling binary. As a consequence, BHs that merge

* E-mail: giacomo.fragione@northwestern.edu

Table 1. Total masses ($m_{\text{BH},1} + m_{\text{BH},2}$) and effective spin (χ_{eff}) of merging BH-BH binaries inferred by the LIGO-Virgo collaboration (LIGO Scientific Collaboration et al. 2019) and the IAS group (Venumadhav et al. 2019; Zackay et al. 2019).

| Group | $m_{\text{BH},1} + m_{\text{BH},2}$ (M_{\odot}) | χ_{eff} |
|------------|---|-------------------------|
| LIGO-Virgo | $18.6^{+6.9}_{-3.9}$ | $0.03^{+0.19}_{-0.07}$ |
| LIGO-Virgo | $21.4^{+11.0}_{-5.7}$ | $0.18^{+0.20}_{-0.12}$ |
| LIGO-Virgo | $36.8^{+19.0}_{-10.3}$ | $0.05^{+0.31}_{-0.20}$ |
| LIGO-Virgo | $50.8^{+12.2}_{-10.2}$ | $-0.04^{+0.17}_{-0.21}$ |
| LIGO-Virgo | $55.8^{+8.4}_{-7.0}$ | $0.07^{+0.12}_{-0.12}$ |
| LIGO-Virgo | $58.8^{+13.4}_{-11.1}$ | $0.08^{+0.17}_{-0.17}$ |
| LIGO-Virgo | $62.1^{+11.8}_{-9.9}$ | $-0.09^{+0.18}_{-0.21}$ |
| LIGO-Virgo | $66.2^{+7.7}_{-7.5}$ | $-0.01^{+0.12}_{-0.13}$ |
| LIGO-Virgo | $68.5^{+17.9}_{-14.5}$ | $0.09^{+0.22}_{-0.26}$ |
| LIGO-Virgo | $84.2^{+25.3}_{-20.3}$ | $0.37^{+0.21}_{-0.25}$ |
| IAS | $23.2^{+8.55}_{-8.55}$ | $0.25^{+0.19}_{-0.19}$ |
| IAS | $23.3^{+6.02}_{-6.02}$ | $0.27^{+0.11}_{-0.11}$ |
| IAS | $39.3^{+9.81}_{-9.81}$ | $0.05^{+0.14}_{-0.14}$ |
| IAS | $44.1^{+9.69}_{-9.69}$ | $-0.16^{+0.21}_{-0.21}$ |
| IAS | $49.7^{+5.94}_{-5.94}$ | $-0.09^{+0.09}_{-0.09}$ |
| IAS | $52.7^{+9.34}_{-9.34}$ | $0.79^{+0.11}_{-0.11}$ |
| IAS | $55.6^{+7.06}_{-7.06}$ | $-0.30^{+0.17}_{-0.17}$ |
| IAS | $55.8^{+4.73}_{-4.73}$ | $0.05^{+0.07}_{-0.07}$ |
| IAS | $59.6^{+7.70}_{-7.70}$ | $0.08^{+0.12}_{-0.12}$ |
| IAS | $62.2^{+6.38}_{-6.38}$ | $-0.05^{+0.12}_{-0.12}$ |
| IAS | $65.1^{+4.84}_{-4.84}$ | $-0.05^{+0.07}_{-0.07}$ |
| IAS | $67.9^{+8.07}_{-8.07}$ | $0.09^{+0.13}_{-0.13}$ |
| IAS | $69.1^{+9.07}_{-9.07}$ | $-0.09^{+0.20}_{-0.20}$ |
| IAS | $74.4^{+10.5}_{-10.5}$ | $0.19^{+0.19}_{-0.19}$ |
| IAS | $76.5^{+15.0}_{-15.0}$ | $0.05^{+0.26}_{-0.26}$ |
| IAS | $78.1^{+11.2}_{-11.2}$ | $-0.63^{+0.23}_{-0.23}$ |
| IAS | $84.6^{+12.5}_{-12.5}$ | $0.43^{+0.13}_{-0.13}$ |

in isolation are expected to enter the LIGO frequency band (10 Hz) almost circular, with typical eccentricities in the range $e_{10\text{Hz}} \sim 10^{-7}-10^{-6}$. In the case the BH binary merges in a hierarchical system as a result of the LK mechanism, a number of authors showed that the typical eccentricity has much higher values, in the range $\sim 10^{-2}-10^{-1}$ (Wen 2003; Antonini et al. 2016; Fragione & Bromberg 2019; Fragione & Kocsis 2019; Fragione & Loeb 2019a). If the BH binary is dynamically assembled in a cluster environment, the spectrum of possible eccentricities is rich, with three possible outcomes (Samsing & D’Orazio 2018; Zevin et al. 2018): (i) binaries that are ejected and merge outside the cluster have eccentricities $\sim 10^{-7}-10^{-6}$, as in the isolated binary case; (ii) binaries that merge as a result of a GW capture process have eccentricities $\sim 10^{-2}-10^{-1}$, as in the LK-induced mergers; (iii) binaries that merge within the cluster have intermediate eccentricities $\sim 10^{-5}-10^{-3}$. The recent non-detection of eccentric sources by LIGO-Virgo was used to place an upper limit on the rate of eccentric mergers with $e_{10\text{Hz}} > 0.1$ of $\mathcal{R} \leq 300 f_{\text{ecc}} \text{Gpc}^{-3}\text{yr}^{-1}$, where f_{ecc} is the fraction of mergers with $e_{10\text{Hz}} > 0.1$ (LIGO Scientific Collaboration et al. 2019). In comparison, the rate density of circular mergers is between $28-104 \text{Gpc}^{-3}\text{yr}^{-1}$ for a power-law mass distribution prior (LIGO Scientific Collaboration et al. 2019). The eccentricity of dynamically formed BH binaries is much higher in the GW frequency band of LISA.

Another powerful quantity to discriminate among the contributions of different astrophysical merger channels is χ_{eff} , the effective spin of the BH binary at merger defined as the mass-weighted average of the binary components’ spins projected onto the orbital angular momentum vector of the binary. Binaries that evolve and merge in isolation are expected to have spin vectors that are aligned with the orbital angular momentum vector of the binary mainly due to tidal dissipation effects (Vitale et al. 2017; Gerosa et al. 2018). BHs that merge in star clusters are instead expected to have spin vectors distributed isotropically, as a consequence of the fact that the dynamical binary assembly does not prefer any specific direction (Rodríguez et al. 2016; Arca Sedda & Benacquista 2019b). For what concerns the focus of this work, LK-induced mergers in triple systems, Antonini et al. (2018) and Rodríguez & Antonini (2018) claimed that the BH binary component spins typically align in the perpendicular direction with respect to the orbital angular momentum of the binary due to the tertiary companion in a triple system, implying near-zero effective spins at merger. However, even more recently, Liu et al. (2019) have shown that these findings are sensitive to the applied approximations and orbit-averaging in the equations of motion. They showed that the BH spin exhibits a wide range of evolutionary paths, and different distributions of final spin-orbit misalignments can be produced depending on the system parameters.

In this paper, we study the dynamical evolution of BH triples by means of high-precision direct N -body simulations, including post-Newtonian (PN) terms up to 2.5PN order. We start from the main sequence progenitors of the BHs and model the supernova (SN) events that lead to the formation of the BH triple. We adopt different prescriptions for the SN natal kicks, and consider different progenitor metallicities and orbital parameters. We determine the expected distributions of various properties of merging systems, including masses, eccentricities, spin-orbit misalignment, and merger times.

The paper is organized as follows. In Section 2, we discuss the initial conditions adopted in this paper. In Section 3, we discuss the distribution of masses, orbital parameters, eccentricities and spin-orbit misalignments of merging systems. Finally, in Section 4, we discuss the implications of our findings and draw our conclusions.

2 INITIAL CONDITIONS

The stellar triples in our simulations are initialized as described in what follows. In total, we consider nine different models (see Table 2).

We consider a triple system comprised of an inner binary of mass $m_{\text{in}} = m_1 + m_2$ and a third body of mass m_3 that orbits the inner binary. The semi-major axis and eccentricity of the inner orbit are a_{in} and e_{in} , respectively, and the semi-major axis and eccentricity of the outer orbit are a_{out} and e_{out} , respectively. The inner and outer orbital plane have initial relative inclination i_0 .

We sample the mass m_1 of the most massive star in the inner binary from an initial mass function

$$\frac{dN}{dm} \propto m^{-\beta}, \quad (1)$$

in the mass range $20 M_{\odot}-150 M_{\odot}$, reflecting the progenitor

Table 2. Models parameters: name, dispersion of BH kick-velocity distribution (σ_{BH}), progenitor metallicity (Z), maximum outer semi-major axis of the triple ($a_{3,\text{max}}$), fraction of stable triple systems after SNe (f_{stable}), fraction of stable systems that merge from the N -body simulations (f_{merge}).

| Name | σ (km s $^{-1}$) | Z | $a_{3,\text{max}}$ (AU) | f_{stable} | f_{merge} |
|------|--------------------------|--------|-------------------------|----------------------|--------------------|
| A1 | 260 | 0.01 | 2000 | 7.8×10^{-5} | 0.06 |
| A2 | 100 | 0.01 | 2000 | 1.5×10^{-3} | 0.06 |
| A3 | 0 | 0.01 | 2000 | 3.1×10^{-2} | 0.08 |
| B1 | 260 | 0.0001 | 2000 | 1.3×10^{-1} | 0.06 |
| B2 | 260 | 0.001 | 2000 | 6.2×10^{-2} | 0.06 |
| B3 | 260 | 0.005 | 2000 | 1.4×10^{-3} | 0.05 |
| B4 | 260 | 0.015 | 2000 | 1.5×10^{-5} | 0.06 |
| C1 | 260 | 0.01 | 5000 | 5.8×10^{-5} | 0.06 |
| C2 | 260 | 0.01 | 7000 | 4.2×10^{-5} | 0.05 |

of the BH. We fix $\beta = 2.3$ (Kroupa 2001). We adopt a flat mass ratio distribution for the inner binary, m_2/m_1 , and the outer binary, $m_3/(m_1 + m_2)$ (Sana et al. 2012; Duchêne & Kraus 2013; Sana 2017). The mass of the secondary in the inner binary and of the third companion are sampled from the range $20 M_{\odot}$ - $150 M_{\odot}$. For comparison, we also estimate how the final rate changes if the mass ratio distribution is assumed to be log-uniform (Sana et al. 2013)¹.

We take the distribution of the inner and outer semi-major axis, a_{in} and a_{out} , respectively, log-uniform Kobulnicky et al. (2014). In order to make sure that the periastron distance of the inner binary is large enough that no common-envelope phase or mass transfer occurs², we set a minimum orbital separation $a_{\text{in}}(1 - e_{\text{in}}^2) \gtrsim 10$ AU (Antonini et al. 2017). We adopt three values for the maximum separation of the triple respectively in different simulation sets, $a_{3,\text{max}} = 2000$ AU, 3000 AU, and 5000 AU, see Table 2 (Sana et al. 2014). For the orbital eccentricities of the inner binary, e_{in} , and outer binary, e_{out} , we assume a flat distribution. The initial mutual inclination i_0 between the inner and outer orbit is drawn from an isotropic distribution, while the other relevant angles (i.e. argument of periastron, argument of node, mean anomaly) are drawn randomly.

After sampling the relevant parameters, we check that the initial configuration satisfies the stability criterion of hierarchical triples of Mardling & Aarseth (2001).

Given this set of initial conditions for the stellar triples, we assume that each of the three stars in the triple undergoes a SN event sequentially. We assume that SNe take place instantaneously (on a time-scale shorter than the orbital period), during which a given star loses mass instantaneously and collapses to a BH (for details see e.g. Pijloo et al. 2012; Toonen et al. 2016; Fragione & Loeb 2019a)³. We determine the final masses of the BHs by using the fitting formulae to the results of the PARSEC stellar evolution code (see Appendix C in Spera et al. 2015). We adopt five different values of the progenitor metallicity as shown in Table 2,

$Z = 0.0001, 0.001, 0.005, 0.01,$ and 0.015 , which ultimately sets the final mass of the BH remnant.

As a result of the mass loss, the exploding star is imparted a kick to its center of mass (Blaauw 1961), and the system receives a natal kick due to recoil from an asymmetric supernova explosion. We assume that the BH natal velocity kick is drawn from a Maxwellian distribution

$$p(v_{\text{k}}) \propto v_{\text{k}}^2 e^{-v_{\text{k}}^2/\sigma^2}, \quad (2)$$

with a velocity dispersion σ . In our fiducial model, we consider $\sigma = 260$ km s $^{-1}$ for NSs, consistent with the distribution deduced by Hobbs et al. (2005). We run an additional model where we set $\sigma = 100$ km s $^{-1}$, consistent with the distribution of natal kicks found by Arzoumanian et al. (2002). We also adopt a model where no natal kick is imparted during BH formation (see Table 2). For BHs, we implement momentum-conserving kicks, in which we assume that the momentum imparted to a BH is the same as the momentum given to a NS (Fryer & Kalogera 2001). As a consequence, the kick velocities for the BHs is lowered by a factor of $1.4 M_{\odot}/m_{\text{BH}}$ with respect to neutron stars. The value of σ is highly uncertain.

After each SN event, the orbital elements of the triple are updated as appropriate (see e.g. Fragione et al. 2019), to account both for mass loss and natal kicks. The final masses of the BHs in the inner binary are $m_{\text{BH},1}$ and $m_{\text{BH},2}$, and the outer companion $m_{\text{BH},3}$. We also check that the stability criterion of hierarchical triples of Mardling & Aarseth (2001) is satisfied and the triple is stable following mass loss and natal kicks. After all the SNe took place, we integrate the triple systems by means of the ARCHAIN code (Mikkola & Merritt 2006, 2008), including PN corrections up to order 2.5PN. We perform ~ 750 - 1000 simulations for each model in Table 2. We fix the maximum integration time as (Sillsbee & Tremaine 2017),

$$T = \min(10^3 \times T_{\text{LK}}, 10 \text{ Gyr}), \quad (3)$$

where T_{LK} is the triple LK timescale (Antognini 2015)

$$T_{\text{LK}} = \frac{8}{15\pi} \frac{m_{\text{tot}}}{m_{\text{BH},3}} \frac{P_{\text{out}}^2}{P_{\text{in}}} (1 - e_{\text{out}}^2)^{3/2}, \quad (4)$$

where $m_{\text{tot}} = m_{\text{BH},1} + m_{\text{BH},2} + m_{\text{BH},3}$ and P_{in} and P_{out} are the inner and outer orbital period, respectively.

¹ From observations, Duchêne & Kraus (2013) found that $f(q) \propto q^{1.16 \pm 0.16}$ and $q^{-0.01 \pm 0.03}$ for solar type stars with period less than or larger than $10^{5.5}$ day, respectively, while Sana et al. (2013) found $f(q) \propto q^{-1.0 \pm 0.4}$ for massive O-type stars.

² This would also shrink the inner orbit and make the LK mechanism strongly suppressed by the relativistic precession (see e.g. Naoz 2016).

³ We ignore the SN-shell impact on the companion stars.

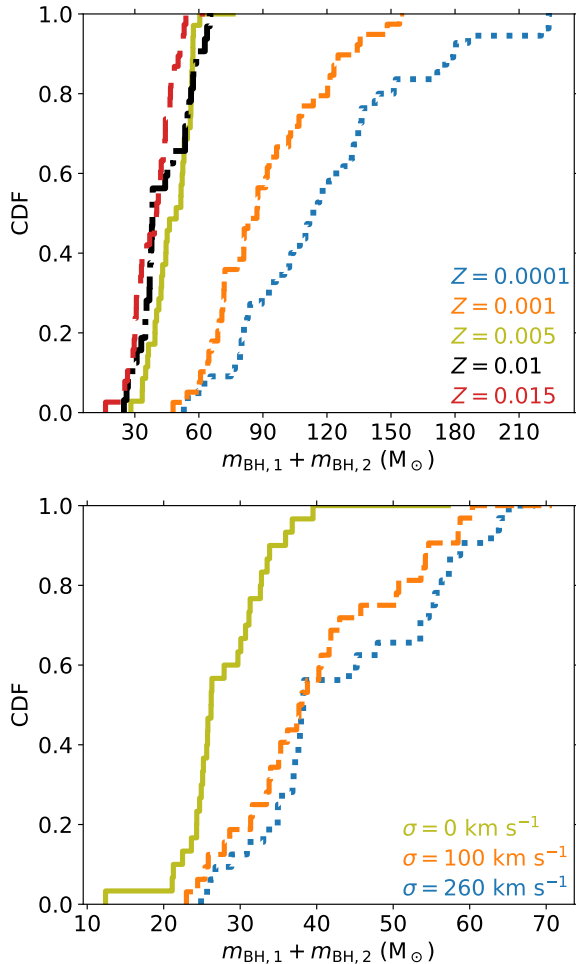


Figure 1. Cumulative distribution function of the total BH mass of BH-BH binaries in triples that lead to a merger, for different values of progenitor metallicity Z (top; $\sigma = 260 \text{ km s}^{-1}$) and σ (bottom; $Z = 0.01$).

3 RESULTS

In our simulations, we find that $\sim 5\%$ – 8% of the triple systems lead to a merger of the inner binary. In the following subsections, we investigate the distribution of these mergers with respect to masses, orbital parameters, and spins.

3.1 Mass distribution

Figure 1 shows the cumulative distribution function (CDF) of the total BH mass of BH-BH binaries in triples that lead to a merger, for different values of Z (top panel; $\sigma = 260 \text{ km s}^{-1}$) and σ (bottom panel; $Z = 0.01$). Both Z and σ affect the distribution of total BH masses.

For $Z \lesssim 0.005$, the distributions do not depend significantly on the progenitor metallicity and the total BH mass is limited to $\sim 60 M_{\odot}$. For higher metallicities, the progenitors can collapse to more massive BHs, up to $\sim 120 M_{\odot}$ – $140 M_{\odot}$ (Spera et al. 2015). We find that $\sim 50\%$ of the mergers have total mass $\gtrsim 90 M_{\odot}$ and $\gtrsim 120 M_{\odot}$ for $Z = 0.001$ and $Z = 0.0001$, respectively. This is consistent with the findings of Fragione & Loeb (2019b). For comparison, we report the

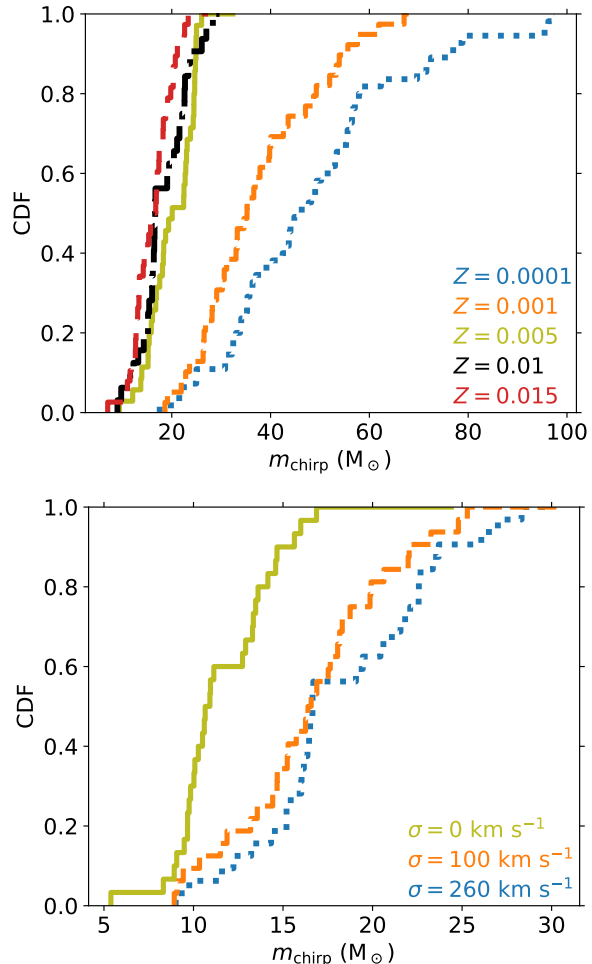


Figure 2. Cumulative distribution function of the chirp mass of BH-BH binaries in triples that lead to a merger, for different values of Z (top panel; $\sigma = 260 \text{ km s}^{-1}$) and σ (bottom panel; $Z = 0.01$).

distribution of total masses inferred from LIGO-Virgo mergers and the IAS group (LIGO Scientific Collaboration et al. 2019; Venumadhav et al. 2019; Zackay et al. 2019) in Table 1. We note that population of very massive binaries we find in our simulations may be due to the fact that we are using fitting formulae to single stellar evolutionary tracks to determine the BH mass from the mass of its progenitor (Spera et al. 2015). We are not modelling the mass loss during neither possible episodes of Roche-lobe overflows nor possible common evolution phases. Nevertheless, we set in our initial conditions a minimum orbital separation $a_{\text{in}}(1 - e_{\text{in}}^2) \gtrsim 10 \text{ AU}$ to ensure that the periastron distance of the inner binary is large enough that no common-envelope phase or mass transfer occurs (Antonini et al. 2017). These processes are modeled in binary systems, but not entirely comprehended in triple systems (Di Stefano 2019; Hamers & Dosopoulou 2019).

Concerning the role of σ , we find that the larger the kick velocity the larger the total BH mass on average. This is explained in relation to our assumption of momentum-conserving kicks, where $\sigma_{\text{BH}} \propto m_{\text{BH}}^{-1}$. In our simulations, for $Z = 0.01$, we find that $\sim 50\%$ of the mergers have

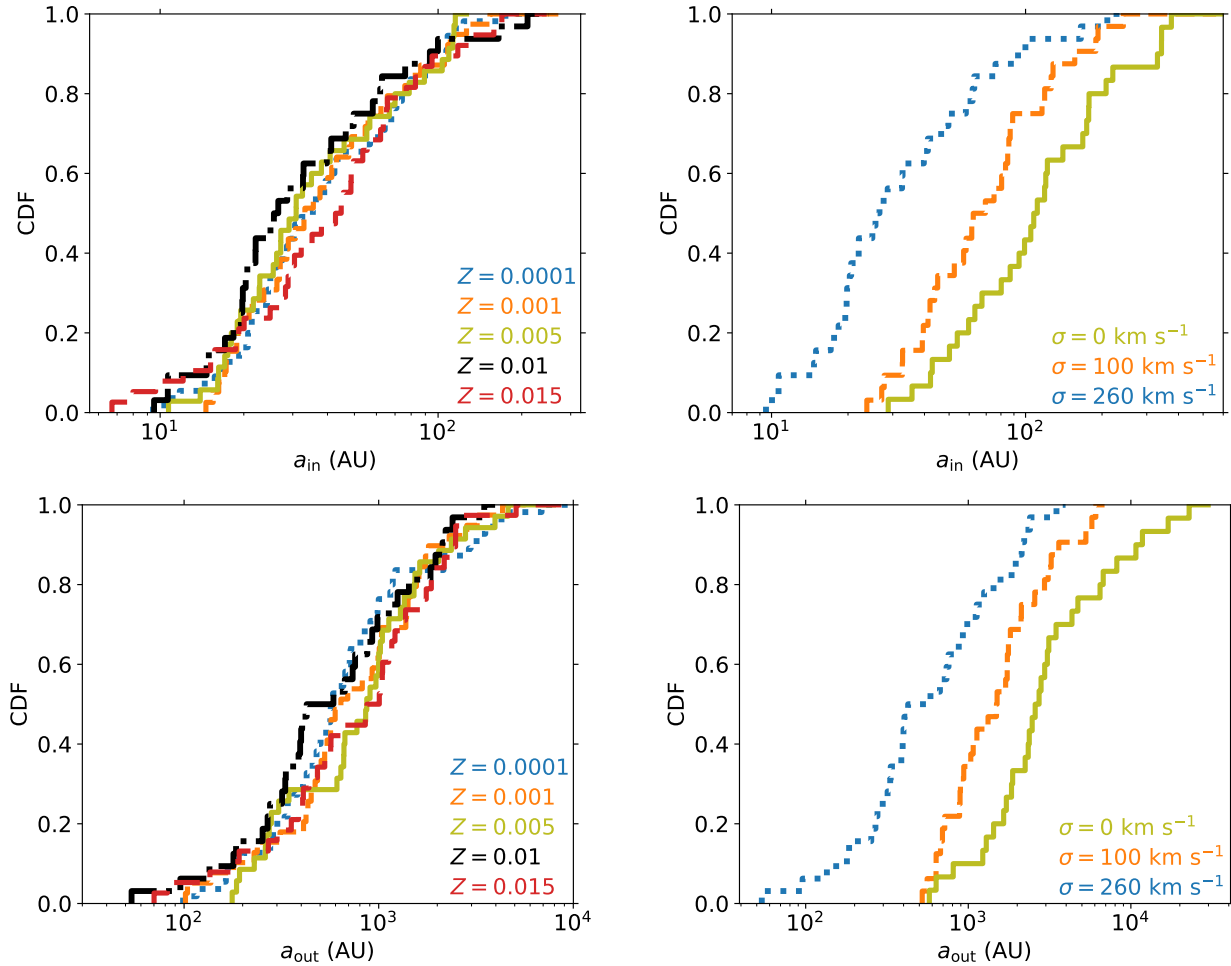


Figure 3. Cumulative distribution function of inner (top) and outer (bottom) semi-major axis of BH-BH binaries in triples that lead to a merger. Left panel: a_{in} and a_{out} for different metallicities Z and $\sigma = 260 \text{ km s}^{-1}$; right panel: a_{in} and a_{out} for different values of σ and $Z = 0.01$.

total mass $\gtrsim 25 M_{\odot}$ and $\gtrsim 40 M_{\odot}$ for $\sigma = 0 \text{ km s}^{-1}$ and $\sigma = 100 \text{ km s}^{-1}$, respectively. Increasing the mean kick velocity to $\sigma = 260 \text{ km s}^{-1}$ does not change considerably the distribution of total masses. Other prescriptions for the natal kicks may lead to different total mass distributions.

We report in Figure 2 the CDF of the chirp mass, the combination of masses measured most accurately during the inspiral,

$$m_{\text{chirp}} = \frac{(m_{\text{BH},1} m_{\text{BH},2})^{3/5}}{(m_{\text{BH},1} + m_{\text{BH},2})^{1/5}}, \quad (5)$$

of BH-BH binaries in triples that lead to a merger, for different values of Z (top panel; $\sigma = 260 \text{ km s}^{-1}$) and σ (bottom panel; $Z = 0.01$). As in the case of the total mass, the distribution of chirp masses is not significantly affected by the progenitor metallicity for $Z \gtrsim 0.005$, $\sim 90\%$ of the BH-BH mergers have $m_{\text{chirp}} \lesssim 20 M_{\odot}$. We also find that $\sim 50\%$ of the mergers have $m_{\text{chirp}} \gtrsim 35 M_{\odot}$ and $m_{\text{chirp}} \gtrsim 45 M_{\odot}$ for $Z = 0.001$ and $Z = 0.0001$, respectively. Moreover, lower natal kicks predict lower chirp masses. We find that $\sim 50\%$ of the BH-BH mergers have $m_{\text{chirp}} \gtrsim 10 M_{\odot}$ and $m_{\text{chirp}} \gtrsim 18 M_{\odot}$ for $\sigma = 0 \text{ km s}^{-1}$ and $\sigma = 100 \text{ km s}^{-1}$, respectively. Furthermore, increasing the mean kick velocity

to $\sigma = 260 \text{ km s}^{-1}$ does not change the distribution of chirp masses significantly. This is consistent with the results of Fragione & Loeb (2019b), who studied the BH-NS mergers in triples.

3.2 Inner and outer semi-major axis

Figure 3 illustrates the CDF of inner (top panel) and outer (bottom panel) semi-major axis of BH-BH binaries in triples that lead to a merger for different values of the progenitor metallicity ($\sigma = 260 \text{ km s}^{-1}$) and mean natal kick velocities ($Z = 0.01$). The progenitor metallicity does not affect the distribution of the inner and outer semi-major axes. On the other hand, the value of σ highly affects their distribution, since higher kicks unbind wider triples. We find that $\sim 50\%$ of the systems have $a_{\text{in}} \lesssim 25 \text{ AU}$, $\lesssim 60 \text{ AU}$, $\lesssim 100 \text{ AU}$ for $\sigma = 0 \text{ km s}^{-1}$, 100 km s^{-1} , 260 km s^{-1} , respectively, and $\sim 50\%$ of the systems have $a_{\text{out}} \lesssim 500 \text{ AU}$, $\lesssim 1500 \text{ AU}$, $\lesssim 2500 \text{ AU}$ for $\sigma = 0 \text{ km s}^{-1}$, 100 km s^{-1} , 260 km s^{-1} , respectively. Similar conclusions were found in Fragione, Leigh, Perna & Kocsis (2019) and Fragione et al. (2019).

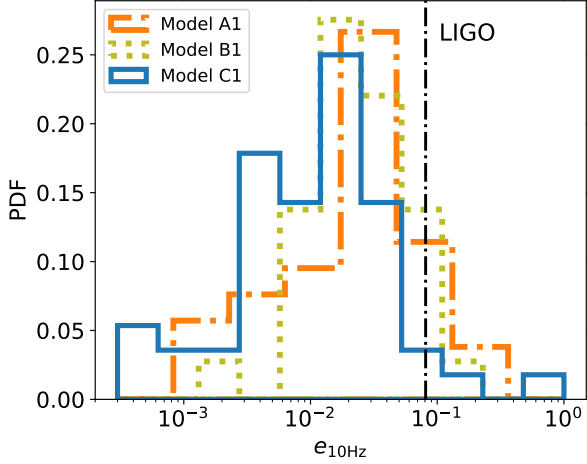


Figure 4. Distribution of eccentricities at the moment the CO binaries enter the LIGO frequency band (10 Hz) for mergers produced by triples. The vertical line shows the conservative minimum $e_{10\text{Hz}} = 0.081$ where LIGO/VIRGO/KAGRA network may distinguish eccentric sources from circular sources (Gondán & Kocsis 2019). Note that for lower mass sources, the detection threshold at design sensitivity is $e_{10\text{Hz}} = 0.023$, see footnote 4).

3.3 Eccentricity

For the BH-BH binaries that merge in our simulations, we compute a proxy for the GW frequency, i.e. the frequency corresponding to the harmonic that gives the maximum GW emission (Wen 2003)

$$f_{\text{GW}} = \frac{\sqrt{G(m_{\text{BH},1} + m_{\text{BH},2})}}{\pi} \frac{(1 + e_{\text{in}})^{1.1954}}{[a_{\text{in}}(1 - e_{\text{in}}^2)]^{1.5}}. \quad (6)$$

In Figure 4, we illustrate the probability distribution function (PDF) of eccentricities at the moment the BH binaries enter the LIGO frequency band, for Models A1, B1 and C1. We also show the minimum eccentricity $e_{10\text{Hz}} = 0.081$ where the LIGO/VIRGO/KAGRA network may distinguish eccentric sources from circular sources (Gondán & Kocsis 2019).⁴ This value is consistent with the recent LIGO/VIRGO analysis (LIGO Scientific Collaboration et al. 2019). A large fraction of merging BH-BH in triples retain a significant eccentricity at 10 Hz, $\sim 42\%$ ($\sim 9\%$) of the merging systems have $e_{10\text{Hz}}$ higher than 0.023 (0.081). We note that a similar signature could be found for BH binaries that merge near supermassive and intermediate-mass black holes (Fragione et al. 2019; Fragione & Bromberg 2019; Fragione et al. 2019), in the GW capture scenario in star clusters (Samsing 2018), and in triple (Antonini et al. 2017) and quadruple (Fragione & Kocsis 2019) systems.

3.4 Spin

In our simulations, we incorporate the spin-orbit coupling effect by introducing the spin vector $\mathbf{S} = S\hat{\mathbf{S}}$, where $S =$

⁴ Note that the detection threshold of $e_{10\text{Hz}}$ varies for different binary mass. For binaries with masses of those in the LIGO observing run O1 and O2, the minimum detectable eccentricity ranges between $e_{10\text{Hz}} = 0.023$ and 0.081 (Gondán & Kocsis 2019).

Table 3. Spin models: name, Kerr parameter of the BH (χ), initial direction of the spins.

| Name | χ | Initial direction |
|------|----------|---|
| S1 | uniform | $0^\circ \leq \cos \theta_{1,2}^{\text{ini}} \leq 20^\circ$ |
| S2 | Eq. (10) | $0^\circ \leq \cos \theta_{1,2}^{\text{ini}} \leq 20^\circ$ |
| T1 | uniform | aligned with \mathbf{J} |
| T2 | uniform | $\cos \theta_{1,2}^{\text{ini}}$ uniform |
| U1 | 0.2 | $0^\circ \leq \cos \theta_{1,2}^{\text{ini}} \leq 20^\circ$ |
| U2 | 0.5 | $0^\circ \leq \cos \theta_{1,2}^{\text{ini}} \leq 20^\circ$ |
| U3 | 0.8 | $0^\circ \leq \cos \theta_{1,2}^{\text{ini}} \leq 20^\circ$ |

$(Gm_{\text{BH}}^2/c)\chi$, where $0 \leq \chi \leq 1$ is the dimensionless Kerr parameter. The leading order (1.5PN) de Sitter precession of the spins \mathbf{S}_1 and \mathbf{S}_2 of the BHs in the inner binary around the inner binary angular momentum \mathbf{J} is given by (Apostolatos et al. 1994)

$$\frac{d\mathbf{S}_1}{dt} = \boldsymbol{\Omega}_1 \times \mathbf{S}_1 = \left[\frac{2G\mu}{c^2 r^3} \left(1 + \frac{3m_2}{4m_1} \right) \mathbf{r} \times \mathbf{v} \right] \times \mathbf{S}_1 \quad (7)$$

$$\frac{d\mathbf{S}_2}{dt} = \boldsymbol{\Omega}_2 \times \mathbf{S}_2 = \left[\frac{2G\mu}{c^2 r^3} \left(1 + \frac{3m_1}{4m_2} \right) \mathbf{r} \times \mathbf{v} \right] \times \mathbf{S}_2, \quad (8)$$

where $\mu = m_1 m_2 / (m_1 + m_2)$ is the inner binary reduced mass, $\mathbf{r} = \mathbf{r}_1 - \mathbf{r}_2$ and $\mathbf{v} = \mathbf{v}_1 - \mathbf{v}_2$.⁵ GW measurements are especially sensitive to the following combination of the two spins (Abbott et al. 2016; Vitale et al. 2017)

$$\chi_{\text{eff}} = \frac{m_{\text{BH},1} \chi_1 \cos \theta_1 + m_{\text{BH},2} \chi_2 \cos \theta_2}{m_{\text{BH},1} + m_{\text{BH},2}}, \quad (9)$$

where $\cos \theta_1 = (\hat{\mathbf{S}}_1 \cdot \mathbf{J})/J$ and $\cos \theta_2 = (\hat{\mathbf{S}}_2 \cdot \mathbf{J})/J$, where \mathbf{J} is the total angular momentum of the inner BH binary, which is well approximated by the orbital angular momentum.

The magnitudes of the BH spins are expected to be set by the physics governing the stellar collapse, which depends on the progenitor star metallicity and mass loss. However, since the specific predictions on how the progenitor properties set the remnant spin is still highly uncertain, therefore we run simulations for seven different models for the spins in order to understand how the results depend on the initial spin of the BHs. Each model differs in the initial magnitude of the Kerr spin parameter and/or the initial orientation of the spins (see Table 3)

- Model S1: χ_1 and χ_2 are drawn independently from an uniform distribution and angles between $0^\circ \leq \cos \theta_{1,2}^{\text{ini}} \leq 20^\circ$,⁶
- Model S2: χ_1 and χ_2 set by the BH mass (Belczynski et al. 2017)

$$\chi_{1,2} = \frac{p_1 - p_2}{2} \tanh \left(p_3 - \frac{M_{\text{BH},1,2}}{M_\odot} \right) + \frac{p_1 + p_2}{2}, \quad (10)$$

where $p_1 = 0.86 \pm 0.06$, $p_2 = 0.13 \pm 0.13$, and $p_3 = 29.5 \pm 8.5$. Following Gerosa et al. (2018), spins are generated by drawing random samples uniformly in the region in between the two curves given by the upper and lower limits of the

⁵ We neglect the backreaction of \mathbf{S}_1 and \mathbf{S}_2 on \mathbf{J} and the spin-spin precessional terms (Antonini et al. 2018; Liu et al. 2019).

⁶ Here $\cos \theta_{1,2} = \hat{\mathbf{S}}_{1,2} \cdot \hat{\mathbf{L}}$ describes the spin misalignment angle relative to the orbital angular momentum vector.

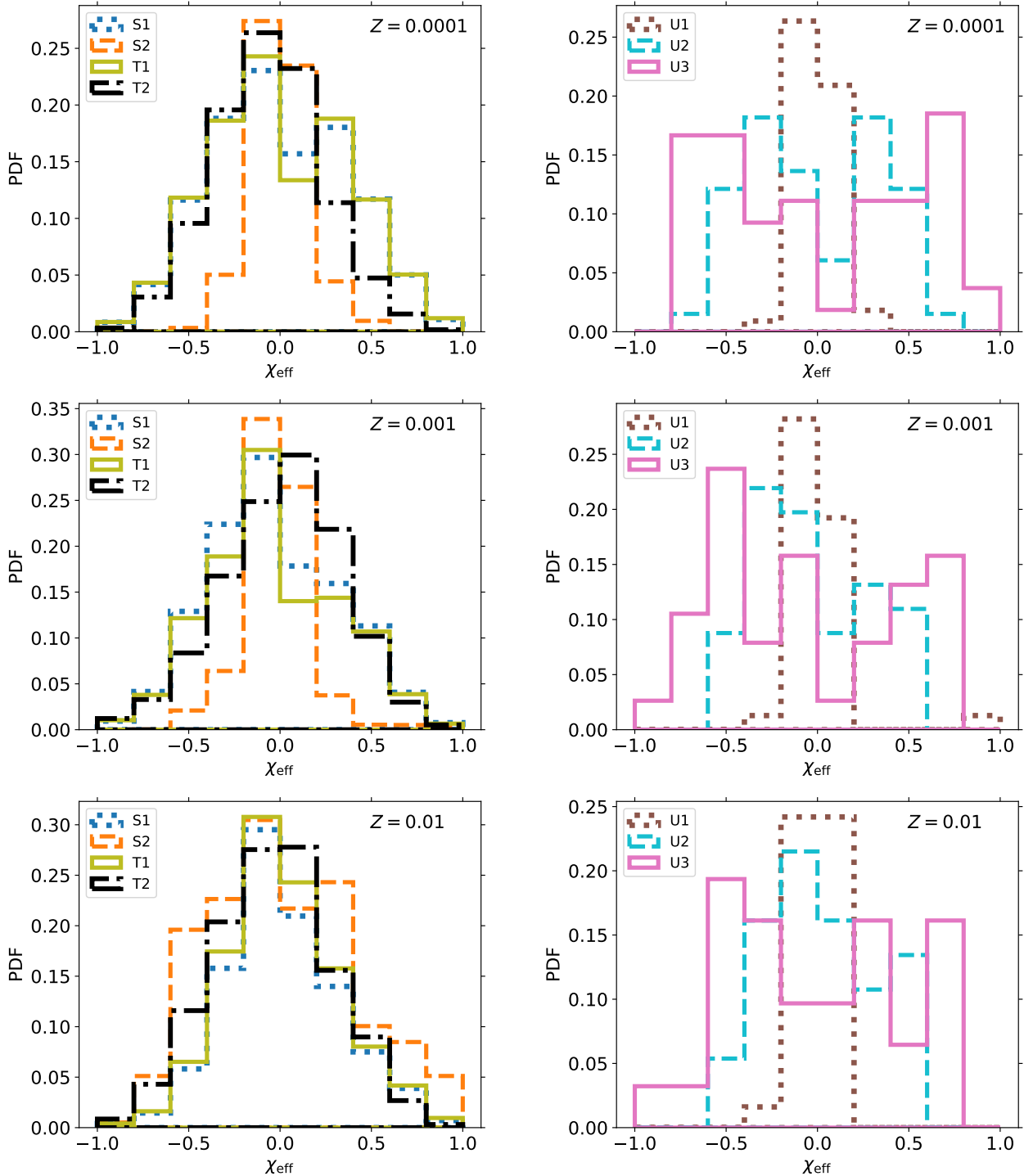


Figure 5. Effective spin distributions of BH-BH binaries in triples that lead to merger for different values of Z (top: Model B1; centre: Model A1; bottom: Model B4) and all the spin models under consideration (see Table 3).

parameters. Eq. 10 captures some of the key features found in Belczynski et al. (2017), that is heavier BHs tend to have smaller spins, and reflects the uncertainties of this model (see e.g. Figure 1 in Gerosa et al. 2018). The misalignment angles are drawn from $0^\circ \leq \cos \theta_{1,2}^{\text{ini}} \leq 20^\circ$ uniformly;

- Model T1: χ_1 and χ_2 are drawn independently from an

uniform distribution and the spins are aligned with the inner angular momentum;

- Model T2: χ_1 and χ_2 are drawn independently from an uniform distribution and the initial spin-orbit misalignments of the BHs are drawn from an isotropic distribution;

- Models U1, U2, U3: χ_1 and χ_2 are fixed at 0.2, 0.5, 0.8, respectively, and $0^\circ \leq \cos \theta_{1,2}^{\text{ini}} \leq 20^\circ$ is drawn uniformly.

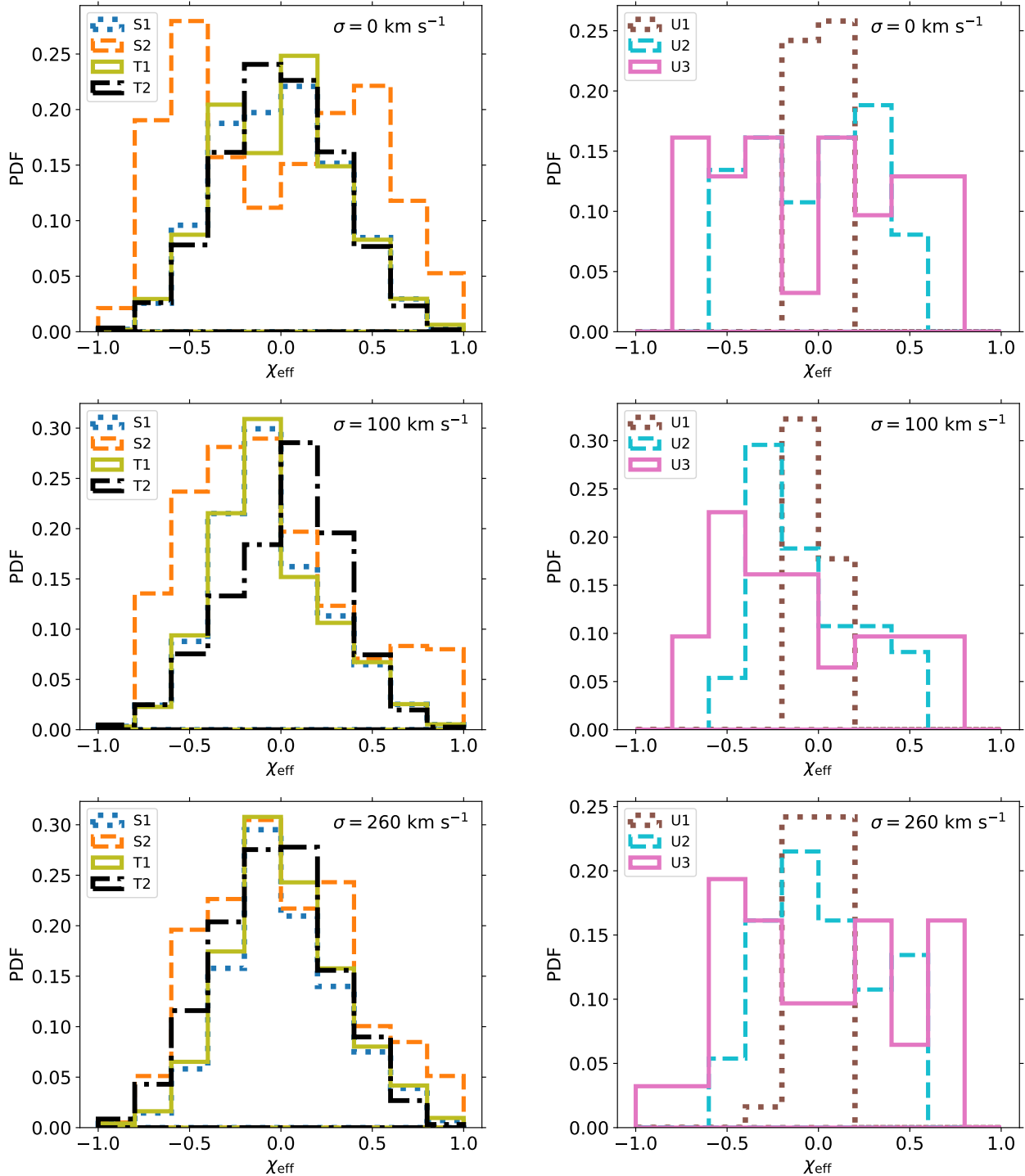


Figure 6. Effective spin distributions of BH-BH binaries in triples that lead to merger for different values of σ (top: Model A3; centre: Model A2; bottom: Model A1) and all the spin models under consideration (see Table 3).

In Figure 5, we show the final χ_{eff} distributions of merging BH-BH binaries in triples for different values of the progenitor metallicity. In the right panel of Figure 5, we show the PDFs of the effective spins for Models U1, U2, and U3, where we fix the initial Kerr parameters of the BHs to 0.2, 0.5, 0.8, respectively. We find that mergers with high BH spins have a broadly distributed χ_{eff} , and mergers with low

absolute spins have χ_{eff} peaked around zero. The distributions do not depend significantly on the value of Z .

In the left panel, we illustrate the PDFs for Models S1, S2, T1, T2, in which the magnitude of initial spins are sampled from a broad distribution (Table 3). For these distributions, the χ_{eff} distributions have a peak at $\chi_{\text{eff}} \sim 0$ and broad tails, which is not significantly affected by the initial

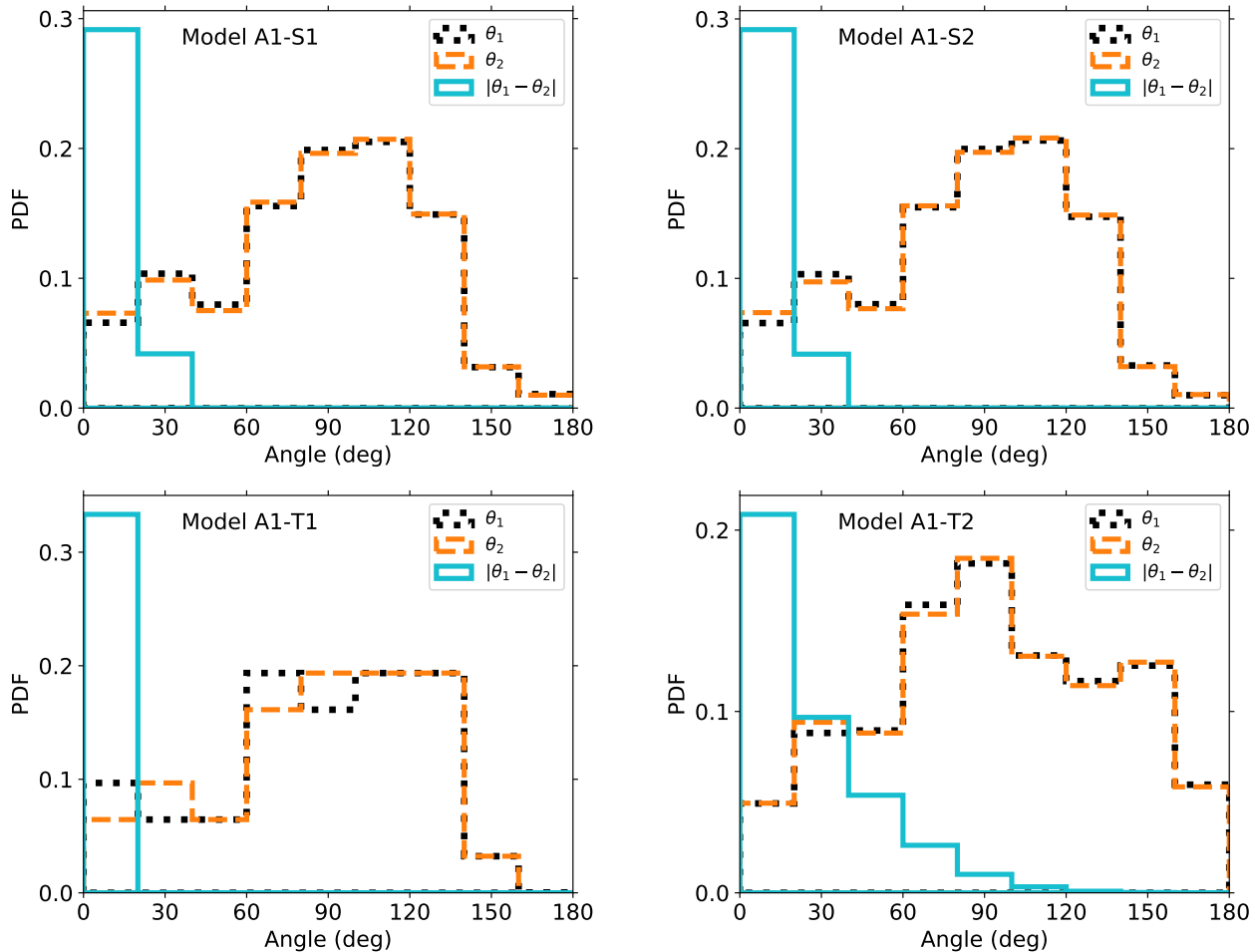


Figure 7. Distributions of the absolute misalignment θ_1 between \mathbf{S}_1 and \mathbf{J} , θ_2 between \mathbf{S}_2 and \mathbf{J} , and the relative misalignment between \mathbf{S}_1 and \mathbf{S}_2 for Model A1 and the first four spin models of Table 3.

distribution of the spins. A possible exception is Model S2 for $Z = 0.0001$ and $Z = 0.001$. In these models, we sample χ_{bh} from Eq. (10). Since low metallicities produce heavy BHs and Eq. (10) implies small initial spins on average, the final PDF results peak at $\chi_{\text{eff}} \sim 0$ with less important tails.

In Figure 6, we show the PDFs of χ_{eff} as a function of σ . The final distributions do not depend significantly on the initial choice of the spins of the BHs in Models S1, S2, T1, T2, and presents a peak at ~ 0 with broad tails. The only outlier is the χ_{eff} distribution in the case $\sigma = 0 \text{ km s}^{-1}$ for Model S2, where the distribution is flatter. In the models where we fix the Kerr parameters, the effective spin PDFs do not depend on σ and present a similar behaviour described above for different Z 's. In Table 1, we report the χ_{eff} inferred from observed BH-BH mergers (LIGO Scientific Collaboration et al. 2019; Venumadhav et al. 2019; Zackay et al. 2019). In general, some of the models are consistent with the observed distributions.

Finally, we show the distributions of the absolute misalignments θ_1 and θ_2 between \mathbf{S}_1 and \mathbf{J} and \mathbf{S}_2 and \mathbf{J} , respectively, and $|\theta_1 - \theta_2|$ in Figure 7. The distributions are similar to each other for the spin Models S1, S2, T1, showing that $|\theta_1 - \theta_2|$ is peaked narrowly at zero, while Model T2 shows a broader tail. Note that this is due to the fact

that the initial orientation of the BH spins were drawn in a correlated way for models S1 and S2 while they are drawn independently from an isotropic distribution in Model T2. The initial correlations may be due to the interaction among progenitor stars, particularly tidal dissipation. Figure 7 shows that the relative orientation of the BH spins do not randomize during the evolution, but they retain the information on the initial conditions. However merging systems in triples do not show counteralignment with $|\theta_1 - \theta_2| > 90^\circ$ irrespective of the initial condition.

We do not find any significant correlation between the spin and the eccentricity in our different models. The only significant correlation is in model S2, where we use Eq. 10. In this case, heavier BHs tend to have smaller spins Belczynski et al. (2017).

3.5 Merger rates

Figure 8 shows the merger time CDFs of BH-BH binaries in triples that lead to merger for different progenitor metallicities (left; $\sigma = 260 \text{ km s}^{-1}$) and different kick velocities and triple orbital parameters (right; $Z = 0.01$). In our simulations, the distribution of merger times does not depend significantly on the progenitor metallicity nor on the possi-

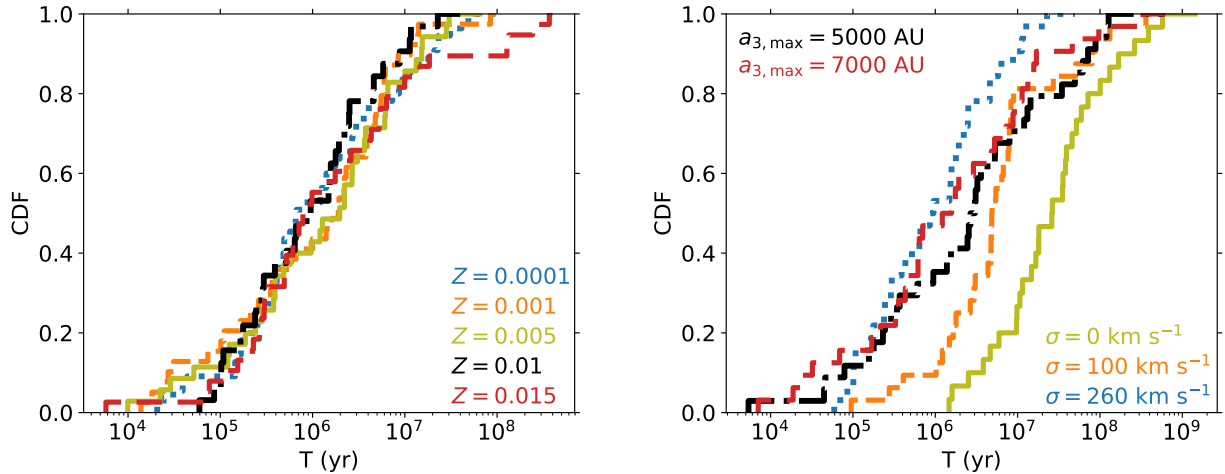


Figure 8. Merger time distribution of BH-BH binaries in triples that lead to merger (see Table 2). Left panel: different progenitor metallicities and $\sigma = 260 \text{ km s}^{-1}$; right panel: different kick velocities and triple orbital parameters and $Z = 0.01$.

ble maximum separation of the triple $a_{3,\text{max}}$. The only parameter on which the merger time depends significantly is the mean kick velocity, since larger values of σ unbind more wider triples. Therefore, triples surviving the SNe are wider for lower σ on average and merge on a longer timescale since their LK timescale is longer.

In order to compute the merger rate of BH-BH binaries in triples, we follow the method outlined in Silsbee & Tremaine (2017) and Fragione et al. (2019). We assume that the local star formation rate is $0.025 \text{ M}_\odot \text{ Mpc}^{-3} \text{ yr}^{-1}$ (Bothwell et al. 2011), thus the number of stars formed per unit mass, volume, and time is given by,

$$\begin{aligned} \dot{n}(m) &= \frac{\eta_{\text{SFR}} f(m)}{\langle m \rangle} = \\ &= 5.2 \times 10^6 \left(\frac{m}{\text{M}_\odot} \right)^{-2.3} \text{ M}_\odot^{-1} \text{ Gpc}^{-3} \text{ yr}^{-1}, \quad (11) \end{aligned}$$

where $\langle m \rangle = 0.38 \text{ M}_\odot$ is the average stellar mass for a Kroupa mass function. Assuming a constant star-formation rate⁷, the BH-BH merger rate in triple systems is then,

$$\begin{aligned} \mathcal{R}_{\text{BH-BH}} &= (1 - \zeta) f_3 f_{\text{stable}} f_{\text{merge}} \int_{20 \text{ M}_\odot}^{150 \text{ M}_\odot} \dot{n}(m_1) dm_1 = \\ &= 7.4 \times 10^4 \eta (1 - \zeta) f_3 f_{\text{stable}} f_{\text{BH-BH}} \text{ Gpc}^{-3} \text{ yr}^{-1}, \quad (12) \end{aligned}$$

where $f_3 = 0.25$ is the fraction of stars in triples, f_{stable} is the fraction of systems that remain stable after the SN events take place, f_{merge} is the fraction of systems that merge (see Table 2), and η is the conditional probability that the secondary is also a progenitor of a BH given that the primary is a BH progenitor:

$$\eta = \frac{\int_{20 \text{ M}_\odot}^{150 \text{ M}_\odot} dm_1 f_{\text{IMF}}(m_1) \int_{20 \text{ M}_\odot/m_1}^1 dq_{12} f_q(q_{12})}{\int_{20 \text{ M}_\odot}^{150 \text{ M}_\odot} dm_1 f_{\text{IMF}}(m_1)}, \quad (13)$$

⁷ The star-formation rate depends on the cosmic time. Rodriguez & Antonini (2018) adopted a redshift-dependent star-formation rate from Madau & Dickinson (2014) and found a similar range for the overall merger rate of triple BHs.

where $f_q(q_{12})$ is the mass ratio distribution of the inner binary, which we assume to be constant. For a Kroupa (2001) initial mass function f_{IMF} we get $\eta = 0.38$. In Eq. (12), $f_{\text{merge}} \sim 0.06$ for all the models, we find that the fraction of stable systems depends both on the mean natal kick and on Z , because lower progenitor metallicities lead to more massive BHs, which are on average imparted lower kicks at birth as a result of our assumption of momentum-conserving kicks (see Tab.2). A factor of uncertainty is the possible KL dynamics during the evolution of the stellar triples before they form a BH-BH system in the inner binary, which we have not modeled here. Some fraction of the parameter space can be removed by the earlier evolution of the system (Shappee & Thompson 2013). To estimate this uncertainty, we assume very conservatively that any stellar triple whose initial KL timescale is less than the lifetime of the primary star (~ 7 Myr; Iben 1991; Hurley et al. 2000; Maeder 2009) in the inner binary will merge, and, as a consequence, will not form a triple system with an inner BH-BH binary (Rodriguez & Antonini 2018). We find that the fraction of these triples is $\zeta \sim 0.83$ on average, except for Model A2 where we find $\zeta \sim 0.55$. Using the minimum and maximum values of f_{stable} in Table 2 and plugging numbers into Eq. (12),

$$\Gamma_{\text{BH-BH}} = 0.008 - 9 \text{ Gpc}^{-3} \text{ yr}^{-1}. \quad (14)$$

This is consistent with the merger rates in triples derived by Antonini et al. (2017) and Silsbee & Tremaine (2017). The higher merger rates correspond to low natal kicks and low progenitor metallicities. For a log-uniform distribution of mass ratios, we estimate a rate ~ 2 times larger.

4 DISCUSSION AND CONCLUSIONS

Many astrophysical scenarios have been proposed to explain the BH and NS mergers observed via GW emission by the LIGO-Virgo collaboration. A promising way to disentangle the contributions from different channels is to statistically compare the distributions of masses, spins, eccentricity and redshift of the merging binaries as discussed in Section 1. In this paper, we have studied the dynamical evolution of BH

triples in isolation by means of high-precision N -body simulations, including post-Newtonian terms up to order 2.5PN. We started from the main sequence progenitors of the BHs and modeled the SNe that lead to the formation of the BH triple. We adopted different prescriptions for the SN natal kicks, and considered different progenitor metallicities and orbital parameters. We have shown that the typical eccentricity of BH-BH binaries merging in triple systems when reaching the 10 Hz is 0.01-0.1 and that the merger rate is in the range $0.02 - 24 \text{ Gpc}^{-3} \text{ yr}^{-1}$, depending on the natal kick prescriptions and progenitor metallicity, consistent with the rates inferred by Antonini et al. (2017) and Silsbee & Tremaine (2017). Higher rates correspond to low natal kicks and low metallicities. We find that the fraction of mergers with a detectable nonzero eccentricity for the LIGO-VIRGO-KAGRA network at design sensitivity is in the range $\sim 9-42\%$.

We confirm the findings of Liu et al. (2019) that the BH spin exhibits a wide range of evolutionary paths, and different distributions of final spin-orbit misalignments can be produced depending on the system parameters. The effective spin parameter χ_{eff} is broadly distributed if the merging BHs are highly spinning. Nevertheless, χ_{eff} is peaked at zero for all triple population models that we have investigated, due to the fact that many merging systems have low intrinsic BH spins in these models, consistent with Antonini et al. (2018) and Rodriguez & Antonini (2018). We have also discussed that the triple scenario we studied in this paper could reproduce the distribution of effective spins inferred from LIGO-Virgo mergers and the IAS group (LIGO Scientific Collaboration et al. 2019; Venumadhav et al. 2019; Zackay et al. 2019).

We note that when we check that the triple systems remain stable after each SN event, systems that are deemed unstable by the Mardling & Aarseth (2001) criterion could still merge, thus possibly enhancing our inferred merger rates. In our calculations, we assumed that the SN events take place instantaneously and do not simulate the systems during the main sequence lifetime of the progenitors. Nevertheless, we have used fits to single stellar evolutionary tracks to determine the final BH mass (Spera et al. 2015). However, the details of the specific evolutionary paths, which depend on stellar winds, metallicity and rotation, of the stellar progenitors could reduce the parameter space (Shappee & Thompson 2013). The situation becomes more complicated if mass loss during possible episodes of Roche-lobe overflows and common evolution phases in the triple are considered (Di Stefano 2019; Hamers & Dosopoulou 2019). We do not model these possible effects and leave the detailed study to future investigations.

Ongoing and future observations promise to observe hundreds of merging BHs, thus providing a sufficiently high number to constrain the different formation scenarios. The GW observation of a merging BH-BH binary which enters the LIGO band with a non-negligible eccentricity and with a nearly zero effective spin would be consistent with triple scenario.

While our results show that the mass-weighted sum of the spin vectors projected on the orbital angular momentum vector, χ_{eff} , is approximately symmetrically distributed around ~ 0 in the triple channel, we find that the angle between the individual spins is strictly less than $\sim 90^\circ$ (Fig-

ure 7). While this parameter is poorly constrained in the O1 and O2 observing runs, it is potentially measurable through the effects of spin-precession in future longer duration detections at lower GW frequencies (see also Khan et al. 2019; Fairhurst et al. 2019). The misalignment angle between the two spins represents a powerful constraint to test the triple channel of BH mergers.

ACKNOWLEDGEMENTS

GF thanks Seppo Mikkola for helpful discussions on the use of the code ARCHAIN, and Barak Zackay for providing data on the effective spins of binary black hole mergers. We thank Fabio Antonini for useful discussions. GF acknowledges support from a CIERA postdoctoral fellowship at Northwestern University. This work received funding from the European Research Council (ERC) under the European Unions Horizon 2020 Programme for Research and Innovation ERC-2014-STG under grant agreement No. 638435 (GalNUC) and from the Hungarian National Research, Development, and Innovation Office under grant NKFIH KH-125675 (to BK). This research was supported in part by the National Science Foundation under Grant No. NSF PHY-1748958.

REFERENCES

- Abbott B. P., Abbott R., Abbott T. D., Abernathy M. R., Acernese F., Ackley K., Adams C., Adams T., Addesso P., Adhikari R. X., et al. 2016, *Physical Review Letters*, 116, 241102
- Antonini J. M. O., 2015, *MNRAS*, 452, 3610
- Antonini F., Chatterjee S., Rodriguez C. L., Morscher M., Pattabiraman B., Kalogera V., Rasio F. A., 2016, *ApJ*, 816, 65
- Antonini F., Perets H. B., 2012, *ApJ*, 757, 27
- Antonini F., Rodriguez C. L., Petrovich C., Fischer C. L., 2018, *MNRAS*, 480, L58
- Antonini F., Toonen S., Hamers A. S., 2017, *ApJ*, 841, 77
- Apostolatos T. A., Cutler C., Sussman G. J., Thorne K. S., 1994, *Physical Review D*, 49, 6274
- Arca Sedda M., Benacquista M., 2019a, *MNRAS*, 482, 2991
- Arca Sedda M., Benacquista M., 2019b, *MNRAS*, 482, 2991
- Arca-Sedda M., Li G., Kocsis B., 2018, *arXiv e-prints*, p. arXiv:1805.06458
- Arzoumanian Z., Chernoff D. F., Cordes J. M., 2002, *ApJ*, 568, 289
- Askar A., Szkudlarek M., Gondek-Rosińska D., Giersz M., Bulik T., 2017, *MNRAS*, 464, L36
- Banerjee S., 2018, *MNRAS*, 473, 909
- Bartos I., Kocsis B., Haiman Z., Márka S., 2017, *ApJ*, 835, 165
- Belczynski K., Holz D. E., Bulik T., O’Shaughnessy R., 2016, *Nature*, 534, 512
- Belczynski K., Klencki J., Meynet G., Fryer C. L., Brown D. A., Chruslinska M., Gladysz W., O’Shaughnessy R., Bulik T., Berti E., 2017, *arXiv e-prints*, p. arXiv:1706.07053
- Blaauw A., 1961, *Bulletin of the Astronomical Institutes of the Netherlands*, 15, 265

- Bothwell M. S., Kennicutt R. C., Johnson B. D., Wu Y., Lee J. C., Dale D., Engelbracht C., Calzetti D., Skillman E., 2011, *MNRAS*, 415, 1815
- Breivik K., Rodriguez C. L., Larson S. L., Kalogera V., Rasio F. A., 2016, *ApJL*, 830, L18
- Cholis I., Kovetz E. D., Ali-Haïmoud Y., Bird S., Kamionkowski M., Muñoz J. B., Raccanelli A., 2016, *Phys. Rev. D*, 94, 084013
- Di Stefano R., 2019, arXiv e-prints, p. arXiv:1903.11618
- D’Orazio D. J., Samsing J., 2018, *MNRAS*, 481, 4775
- Duchêne G., Kraus A., 2013, *Annual Review of Astronomy and Astrophysics*, 51, 269
- Fairhurst S., Green R., Hannam M., Hoy C., 2019, arXiv e-prints, p. arXiv:1908.00555
- Farr B., Holz D. E., Farr W. M., 2018, *ApJL*, 854, L9
- Fishbach M., Holz D. E., Farr B., 2017, *ApJL*, 840, L24
- Fragione G., Bromberg O., 2019, *MNRAS*, 488, 4370
- Fragione G., Grishin E., Leigh N. W. C., Perets H. B., Perna R., 2019, *MNRAS*, 488, 47
- Fragione G., Kocsis B., 2018, *Phys Rev Lett*, 121, 161103
- Fragione G., Kocsis B., 2019, *MNRAS*, 486, 4781
- Fragione G., Leigh N. W. C., Perna R., 2019, *MNRAS*, 488, 2825
- Fragione G., Leigh N. W. C., Perna R., Kocsis B., 2019, *MNRAS*, 489, 727
- Fragione G., Loeb A., 2019a, *MNRAS*, 486, 4443
- Fragione G., Loeb A., 2019b, arXiv e-prints, p. arXiv:1907.08614
- Fragione G., Metzger B. D., Perna R., Leigh N. W. C., Kocsis B., 2019, arXiv e-prints, p. arXiv:1908.00987
- Fryer C. L., Kalogera V., 2001, *ApJ*, 554, 548
- Gerosa D., Berti E., O’Shaughnessy R., Belczynski K., Kesden M., Wysocki D., Gladysz W., 2018, *Phys. Rev. D*, 98, 084036
- Gondán L., Kocsis B., 2019, *ApJ*, 871, 178
- Gondán L., Kocsis B., Raffai P., Frei Z., 2018, *ApJ*, 860, 5
- Grishin E., Perets H. B., Fragione G., 2018, *MNRAS*, 481, 4907
- Hamers A. S., Dosopoulou F., 2019, *ApJ*, 872, 119
- Hamilton C., Rafikov R. R., 2019, arXiv e-prints, p. arXiv:1907.00994
- Hobbs G., Lorimer D. R., Lyne A. G., Kramer M., 2005, *MNRAS*, 360, 974
- Hurley J. R., Pols O. R., Tout C. A., 2000, *MNRAS*, 315, 543
- Iben Jr. I., 1991, *ApJS*, 76, 55
- Inayoshi K., Tamanini N., Caprini C., Haiman Z., 2017, *Phys. Rev. D*, 96, 063014
- Khan S., Chatziioannou K., Hannam M., Ohme F., 2019, *Phys. Rev. D*, 100, 024059
- Kobulnicky H. A., Kiminki D. C., Lundquist M. J., Burke J., Chapman J., Keller E., Lester K., Rolen E. K., Topel E., Bhattacharjee A., Smullen R. A., Vargas Álvarez C. A., Runnoe J. C., Dale D. A., Brotherton M. M., 2014, *The Astrophysical Journal Supplement Series*, 213, 34
- Kocsis B., Suyama T., Tanaka T., Yokoyama S., 2018, *The Astrophysical Journal*, 854, 41
- Kremer K., Chatterjee S., Breivik K., Rodriguez C. L., Larson S. L., Rasio F. A., 2018, *Physical Review Letters*, 120, 191103
- Kroupa P., 2001, *MNRAS*, 322, 231
- Kruckow M. U., Tauris T. M., Langer N., Kramer M., Izard R. G., 2018, *MNRAS*, 481, 1908
- LIGO Scientific Collaboration Virgo Collaboration et al. 2019, *Physical Review X*, 9, 031040
- LIGO Scientific Collaboration Virgo Collaboration Salemi F., 2019, arXiv e-prints, p. arXiv:1907.09384
- Liu B., Lai D., 2017, *ApJL*, 846, L11
- Liu B., Lai D., 2018, *ApJ*, 863, 68
- Liu B., Lai D., 2019, *MNRAS*, 483, 4060
- Liu B., Lai D., Wang Y.-H., 2019, arXiv e-prints, p. arXiv:1905.00427
- Lopez Jr. M., Batta A., Ramirez-Ruiz E., Martinez I., Samsing J., 2018, arXiv e-prints
- Madau P., Dickinson M., 2014, *ARA& A*, 52, 415
- Maeder A., 2009, *Physics, Formation and Evolution of Rotating Stars*
- Mandel I., Farr W. M., Colonna A., Stevenson S., Tiño P., Veitch J., 2017, *MNRAS*, 465, 3254
- Mardling R. A., Aarseth S. J., 2001, *MNRAS*, 321, 398
- Meiron Y., Kocsis B., Loeb A., 2017, *ApJ*, 834, 200
- Mikkola S., Merritt D., 2006, *MNRAS*, 372, 219
- Mikkola S., Merritt D., 2008, *AJ*, 135, 2398
- Naoz S., 2016, *ARA& A*, 54, 441
- Ng K. K. Y., Vitale S., Zimmerman A., Chatziioannou K., Gerosa D., Haster C.-J., 2018, *Phys. Rev. D*, 98, 083007
- Nishizawa A., Berti E., Klein A., Sesana A., 2016, *Phys. Rev. D*, 94, 064020
- Nishizawa A., Sesana A., Berti E., Klein A., 2017, *MNRAS*, 465, 4375
- O’Leary R. M., Kocsis B., Loeb A., 2009, *MNRAS*, 395, 2127
- O’Leary R. M., Meiron Y., Kocsis B., 2016, *ApJLett*, 824, L12
- O’Leary R. M., Rasio F. A., Fregeau J. M., Ivanova N., O’Shaughnessy R., 2006, *The Astrophysical Journal*, 637, 937
- Perna R., Wang Y.-H., Farr W. M., Leigh N., Cantiello M., 2019, *ApJL*, 878, L1
- Pijloo J. T., Caputo D. P., Portegies Zwart S. F., 2012, *MNRAS*, 424, 2914
- Postnov K., Kuranov A., 2017, arXiv e-prints
- Rasskazov A., Kocsis B., 2019, arXiv e-prints, p. arXiv:1902.03242
- Rodriguez C. L., Amaro-Seoane P., Chatterjee S., Rasio F. A., 2018, *PRL*, 120, 151101
- Rodriguez C. L., Antonini F., 2018, *ApJ*, 863, 7
- Rodriguez C. L., Zevin M., Pankow C., Kalogera V., Rasio F. A., 2016, *ApJ*, 832, L2
- Samsing J., 2018, *Phys. Rev. D*, 97, 103014
- Samsing J., D’Orazio D. J., 2018, *MNRAS*, 481, 5445
- Samsing J., D’Orazio D. J., Askar A., Giersz M., 2018, arXiv e-prints
- Samsing J., D’Orazio D. J., Kremer K., Rodriguez C. L., Askar A., 2019, arXiv e-prints, p. arXiv:1907.11231
- Sana H., 2017, in Eldridge J. J., Bray J. C., McClelland L. A. S., Xiao L., eds, *The Lives and Death-Throes of Massive Stars Vol. 329 of IAU Symposium, The multiplicity of massive stars: a 2016 view*. pp 110–117
- Sana H., et al., 2012, *Science*, 337, 444
- Sana H., et al., 2013, *A& A*, 550, A107
- Sana H., Le Bouquin J. B., Lacour S., Berger J. P., Duvert G., Gauchet L., Norris B., Olofsson J., Pickel D., Zins G.,

- Absil O., de Koter A., Kratter K., Schnurr O., Zinnecker H., 2014, *The Astrophysical Journal Supplement Series*, 215, 15
- Schröder S. L., Batta A., Ramirez-Ruiz E., 2018, *ApJL*, 862, L3
- Shappee B. J., Thompson T. A., 2013, *ApJ*, 766, 64
- Silberbein K., Tremaine S., 2017, *ApJ*, 836, 39
- Spera M., Mapelli M., Bressan A., 2015, *MNRAS*, 451, 4086
- Stevenson S., Berry C. P. L., Mandel I., 2017, *MNRAS*, 471, 2801
- Stevenson S., Ohme F., Fairhurst S., 2015, *ApJ*, 810, 58
- Stone N. C., Metzger B. D., Haiman Z., 2017, *MNRAS*, 464, 946
- Tagawa H., Haiman Z., Kocsis B., 2019, arXiv e-prints, p. arXiv:1912.08218
- Tagawa H., Saitoh T. R., Kocsis B., 2018, *PRL*, 120, 261101
- Talbot C., Thrane E., 2017, *Phys. Rev. D*, 96, 023012
- Toonen S., Hamers A., Portegies Zwart S., 2016, *Computational Astrophysics and Cosmology*, 3, 6
- Venumadhav T., Zackay B., Roulet J., Dai L., Zaldarriaga M., 2019, arXiv e-prints, p. arXiv:1904.07214
- Vitale S., Lynch R., Raymond V., Sturani R., Veitch J., Graff P., 2017, *Phys. Rev. D*, 95, 064053
- Vitale S., Lynch R., Sturani R., Graff P., 2017, *Classical and Quantum Gravity*, 34, 03LT01
- Wen L., 2003, *ApJ*, 598, 419
- Yang Y., Bartos I., Gayathri V., Ford S., Haiman Z., Klimentenko S., Kocsis B., Márka S., Márka Z., McKernan B., O’Shaughnessy R., 2019, arXiv e-prints, p. arXiv:1906.09281
- Yang Y., Bartos I., Haiman Z., Kocsis B., Márka Z., Stone N. C., Márka S., 2019, *The Astrophysical Journal*, 876, 122
- Zackay B., Venumadhav T., Dai L., Roulet J., Zaldarriaga M., 2019, *Phys. Rev. D*, 100, 023007
- Zaldarriaga M., Kushnir D., Kollmeier J. A., 2018, *MNRAS*, 473, 4174
- Zevin M., Pankow C., Rodriguez C. L., Sampson L., Chase E., Kalogera V., Rasio F. A., 2017, *ApJ*, 846, 82
- Zevin M., Samsing J., Rodriguez C., Haster C.-J., Ramirez-Ruiz E., 2018, arXiv:1810.00901